Analysis of $I-V$ characteristics of Si diodes irradiated with short-range ions

© V. Eremin, N. Fadeeva, D. Mitina, E. Verbitskaya

Ioffe Institute,
194021 St. Petersburg, Russia

E-mail: elena.verbitskaya@mail.ioffe.ru

Received November 17, 2022
Revised November 22, 2022
Accepted for publication November 22, 2022

Radiation degradation of Si ion detectors becomes critical for the experiments at new facilities giving the beam intensity increase up to 10^5 times. The study is focused on the impact of heavily damaged Bragg peak region (BPR) at the ion range end on the bulk current of Si sensors irradiated with 53.4 MeV ^{40}Ar ions in the fluence range $(1-4) \cdot 10^9$ ion/cm^2. It is shown that taking into account only the generation current component is insufficient to explain the experimental $I-V$ curves. Simulating $I-V$ characteristics and the electric field profiles demonstrated arising of a built-in junction in the BPR, which controls hole diffusion at voltages below full depletion voltage. Contribution of this component to the total diode current enabled the agreement between experimental and simulated $I-V$ curves.

Keywords: silicon sensors, radiation degradation, current-voltage characteristic, carrier diffusion.

DOI: 10.21883/SC.2022.11.54964.4227

1. Introduction

Silicon detectors are widely used in the largest detecting systems in accelerator complexes such as High−Luminosity Large Hadron Collider (HL−LHC) at CERN, Relativistic Heavy Ion Collider (Brookhaven National Laboratory, USA) and the ion acceleration facility at Helmholtz Centre for Heavy Ion Research (GSI, Germany). One of the key features of these facilities is the huge energy of accelerated particles ranging from hundreds of GeV to 14 TeV. At such energies, the range of particles r_p is far larger than the detector thickness d, and they traverse the whole detector thickness and generate practically uniform distribution of radiation-induced defects (point defects and clusters) across the structure thickness, and the silicon properties in the entire bulk deteriorate uniformly. The degradation of Si sensors irradiated with hadrons, such as 23 GeV protons and 1 MeV neutrons (hereafter referred to as „hadrons"), and with MeV electrons has been comprehensively studied during the 20 years period of LHC development, construction, assembling and commissioning. The results on the defect introduction, the properties of the detector sensitive region, the bulk generation current, the electric field profiles and the signal formation allowed building the detector operational scenario within several years device exploiting in the experiments at LHC, as a basis for planning the experiments, the data treatment and equipment maintenance. The majority of experimental results and physical models for fluence dependences of the dark current, carrier transport parameters and the detector signal were summarized in [1]. At present, new types of Si detectors are implemented into the experiments at HL−LHC and studied within the scenario of the most powerful accelerator proposed for the post-LHC era, the Future Circular Collider with an irradiation dose up to $8 \cdot 10^{17}\,\mathrm{n_{eq}/cm^2}$ [1,2].

Nuclear physics also requires the beams of larger and larger intensities. The new facility, which is under construction at GSI within the frame of the Facility for Antiproton and Ion Research (FAIR) international program, should provide an increase in ion beam intensity by up to a factor of 10^5 over the current level. The facility at Joint Institute of Nuclear Research (Dubna, Russia) planned for the future project Dubna Electron−Radioactive Ion Collider fAcility, DERICA, will give extraordinary intensity of radioactive isotopes beams in a wide range of masses and charges [3,4], and both will advance the experimental resources. The thickness of Si devices thus exposed to ion radiation ranges from tens of micrometers for dE/dx detectors, to centimeters for high-resolution calorimeters. The distribution of arising defects along the range to a great extent depends on the ion energy and mass [5]. Degradation of Si detectors exposed to ions producing almost uniform damage over the whole device thickness has been studied by comparing the impact of radiation on 300 μm thick Si detectors with 1.62 GeV ^{40}Ar ions (ion range $r_p \sim 1$ mm) or 23 GeV protons [6]. The results showed that the approaches developed earlier for description of Si detector degradation under hadron irradiation could be extended to ion exposure by introducing a scaling coefficient for the parameterization of the main characteristics.

Detection of short-range ions using Si detectors (r_p is less than the sensor thickness d) is a special point for low-energy nuclear physics, in which Si ion telescopes are the tools of high priority. The telescopes combine dE/dx detector and the ion calorimeter built from several thick Si detectors providing absorption of the whole energy of detected ions. Such ions generate a nonuniform distribution

of damage described by the Bragg curve with a pronounced peak of primary defects (the so-called Bragg peak) in the silicon bulk, and therefore the factors affecting the detector characteristics differ from those for hadron irradiation.

The damage produced by short-range ions includes point defects and clusters, and the latter are concentrated mainly at the end of r_p. Earlier studies in this field were focused on the needs of ion implantation technology [5], and the results concerned mainly to the residual defects after implantation to relatively high ion doses and the profile of ion rearranging under annealing at elevated temperatures. The impact of ion irradiation on the sensor current increase for ion ranges smaller than d was analyzed in [7] for Si detectors irradiated with ^{16}O, ^{40}Ar and ^{110}Xe ions with the energy of few to several tens of MeV as the dependence of the current on fluence. The current-related damage factor α that defines the proportionality between the increase in detector current and fluence (the current degradation rate) was found to be proportional to the averaged nuclear stopping power and equaled $10^{-13}-10^{-12}$ A/cm, whereas for hadrons irradiating Si detectors this value was $4 \cdot 10^{-17}$ A/cm only [8]. However, in [7] the details of the current origin in the nonuniformly damaged region differentiating the contributions from its various parts and clarifying an enhanced α in terms of semiconductor device physics were beyond consideration.

The goal of the study is to identify the features in $I-V$ characteristics and the electric field profile related to the nonuniform defect distribution in Si diodes irradiated with short-range ^{40}Ar ions generating the Bragg peak fairly separated from the p^+-n junction via the analysis of the experimental $I-V$ and $C-V$ data and simulations, and thus disclose the factors affecting the current-related damage rate.

2. Samples and experimental procedure

The experiment was carried out using a set of Si diodes irradiated with 53.4 MeV ^{40}Ar ions. The samples were processed on the n-type Czochralski silicon wafers with the oxygen concentration $[\mathrm{O}] \sim 10^{17}\,\mathrm{cm}^{-3}$ and a resistivity ρ of $60\,\Omega \cdot \mathrm{cm}$, which corresponds to a phosphorus atom concentration N_0 of $7.1 \cdot 10^{13}\,\mathrm{cm}^{-3}$. The p^+ and n^+-contacts were layers doped with boron and phosphorus atoms, respectively, to the concentrations of about $10^{19}\,\mathrm{cm}^{-3}$. The sample thickness d and the p^+-n junction area S were $300\,\mu$m and $0.23\,\mathrm{cm}^2$, respectively. The topology of the p^+-side included the pad p^+-contact surrounded by rings, a p^+-guard ring (inner ring) and three p^+-floating rings that stabilized $I-V$ characteristics by sequential reducing the ring potentials towards the sample edge. Silicon with a rather low resistivity was chosen to manipulate the compensation of the bulk within the ion range and to get a detailed dependence of the diode current on the space charge region (SCR) width W.

Irradiation was carried out at the U-120 cyclotron of the Ioffe Institute, St. Petersburg, Russia, with ^{40}Ar ions with three fluences: $F_1 = 1 \cdot 10^9$, $F_2 = 2 \cdot 10^9$ and $F_3 = 4 \cdot 10^9\,\mathrm{cm}^{-2}$. The profile of the beam intensity over the area of irradiated samples was uniform, and the dose rate was about $2 \cdot 10^7\,\mathrm{cm}^{-2} \cdot \mathrm{s}^{-1}$.

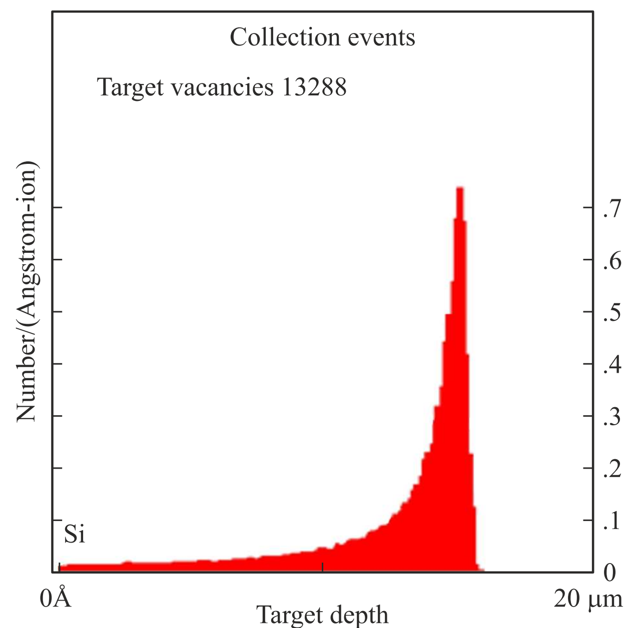

Figure 1. Distribution of primary vacancies along the ion range.

The $I-V$ and $C-V$ measurements were performed at the temperature T of 20°C at bias voltages in the range 0–100 V and with the diode guard ring grounded to minimize the leakage outside the active area of a sample. $I-V$ characteristics were measured with a Keithley 487 picoammeter. The measurements of $C-V$ characteristics were carried out using an Agilent 4263B LCR-meter operated in the parallel mode, and the AC-voltage was 0.5 V.

3. Simulation of collisions events

Collision events arising in a silicon diode irradiated with 53.4 MeV ^{40}Ar ions were simulated using the Stopping and Range of Ions in Matter (SRIM) software [9], which was carried out in the 2D geometry for 5000 ions incident to the same point $x = 0$ (where x is the coordinate along the diode depth) normally to the sample surface. At such ion energy, the dependence of the energy loss dE/dx over the penetration depth represents the Bragg curve with a pronounced peak shortly before the particles stop at approximately $15\,\mu$m from the p^+-contact. Obviously, for any ion hit point at the surface, the statistics of trajectories and ion ranges is the same.

The same simulation also provides the averaged distribution of primary defects (namely, vacancies) along an individual track. For this, the program sums up the number of defects in each layer with a thickness of 1 Å, which gives the distribution of the linear density of defects averaged over

the number of simulated events. The distribution of primary vacancies $N_v(x)$ defined as the average number of vacancies generated by an individual ion at a depth x over a length of 1 Å is presented in the histogram in Fig. 1. The average number of vacancies created by a single ion is 13288, and the Bragg peak maximum lies at $x = r_p = 15.2\,\mu$m. Within the BPR, the maximal introduction rate of vacancies g_V is $7 \cdot 10^7\,\text{cm}^{-1}$ per ion, that is up to 70 times larger than that at the beginning of the range. The local concentration of vacancies $N_V(x)$ is proportional to the fluence.

4. Experimental characteristics of irradiated diodes

4.1. $C-V$ characteristics

$C-V$ characteristics were measured for nonirradiated and irradiated diodes. As shown earlier [10,11], the capacitance of irradiated Si diodes, whose bulk is enriched with deep energy levels (DLs), depends on the frequency f of the probing AC-signal. The dependence is associated with two factors: an increased time constant of the DL filling with free carriers that becomes comparable with the probing signal period, and a lowering the conductivity of the nondepleted part of the damaged region acting as an additional series RC circuit. For both factors, the influence of f on the measured capacitance is more pronounced at higher f and F. Therefore $C-V$ characteristics of the diodes were initially measured at different frequencies of 10, 20 and 100 kHz, and the criterion for choosing the proper f was the minimal difference of the capacitance at the same V with various f. At the maximal fluence F_3, $C-V$ dependences recorded at 10 and 20 kHz were the same, and thereby all $C-V$ measurements were carried out at $f = 20$ kHz (Fig. 2).

Replotting $C-V$ data as C^{-2} vs. V curves yielded the built-in voltage $V_{bi} = (0.6 \pm 0.05)$ V for all irradiated samples. $C-V$ characteristic for the sample irradiated to F_1 matches the curve for the nonirradiated diode, which implies an insignificant change in the effective space charge concentration N_{eff} within the entire damaged region. For the diodes irradiated to F_2 and F_3, the impact of irradiation is noticeable, and the reduction in capacitance of diodes with respect to that of the nonirradiated sample is within 10% at $V = 1-5$ V. This points that in the initial part of ion range the concentration of radiation-induced defects is about $10^{13}\,\text{cm}^{-3}$. At higher V of 5–13 V, the region with a sequential drop and rise in capacitance is observed, and the higher the fluence, the greater the effect.

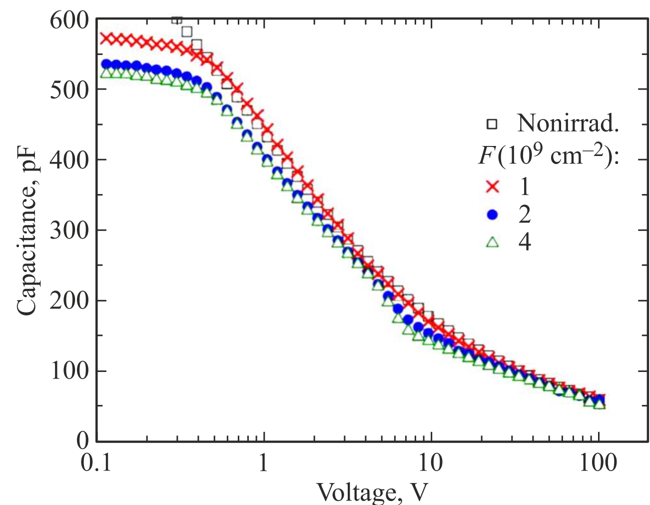

Figure 2. $C-V$ characteristics of Si dioded irradiated to different F. $f = 20$ kHz.

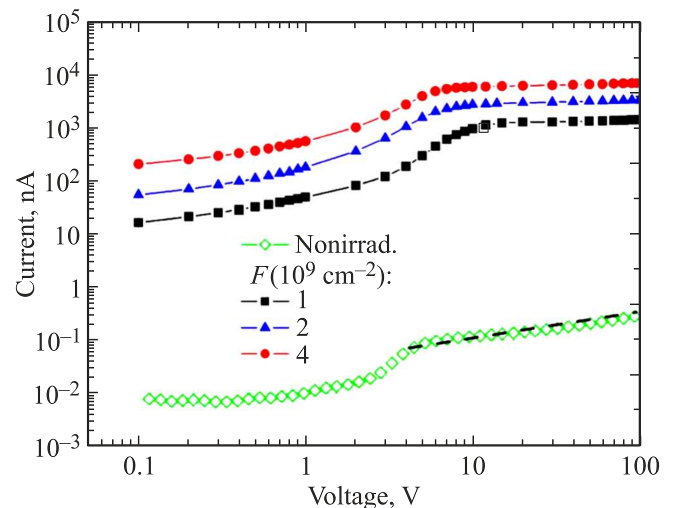

Figure 3. $I-V$ characteristics of nonirradiated and irradiated diodes. Dash line shows a slope $I \sim \sqrt{V}$ corresponding to the region of generation current for the nonirradiated diode.

4.2. $I-V$ characteristics

Fig. 3 shows the dependences of the bulk current on bias voltage for nonirradiated and irradiated diodes. For the latter, the measurements were taken after beneficial annealing the samples at 60°C during 80 min following a procedure of the defect stabilization accepted at CERN-RD50 collaboration for the study of radiation effects in Si detectors irradiated with hadrons. The characteristic of the nonirradiated diode shows three regions, diffusion current at $V < 1$ V, a rather fast increasing current between 2 and 3 V, and a thermally generated current I_g in the depletion region proportional to $\sqrt{V}$ at $V > 4$ V. The origin of the second region is related to the electric field expansion into the gap between the pad electrode and the first p^+-ring, in which SiO_2 layer passivating the gap is overlapped by the pad metallization. The additional area of $\sim 0.1\,\text{mm}^2$ increases the capacitance only slightly; however, it generates extra current at the interface due to a smaller surface recombination time in respect of its value in the bulk.

$I-V$ dependences of irradiated diodes also demonstrate three regions in the current rise to a few μA, which is more than four orders larger than that in the nonirradiated diode. The first region displays a moderate slope of the current rise at $V \leq 1$ V, and then it softly passes to the second one with a larger slope extending to 7−10 V. In accordance with the damage profile (Fig. 1), these regions can be associated with the distribution of radiation-induced defects along the ion range and are preliminary assigned to the current rise in the Low-Damaged Region, LDR (a moderate slope), and in the BPR (a larger slope). The third region can be attributed to the Non-Damaged Region (NDR), in which an insignificant current rise evidences that only the damaged region contributes to the current, whereas the current arising in the NDR is much less due to a large carrier lifetime (a few ms) in the raw silicon. Unlike the nonirradiated diode, for irradiated diodes the tendency to the current saturation suggests that the damaged region is fully depleted at bias voltages above V_{fddr} (where V_{fddr} is the full depletion voltage of the damaged region). The values determined as the voltage corresponding to the intersection point of two lines, the current increase and further slow rise are 12, 9 and 7 V for F_1, F_2 and F_3, respectively. The rise in current at $V > V_{fddr}$ is presumably related to the ohmic leakage.

5. Processing and analysis of the experimental data

5.1. Processing the experimental data and calculation of $I-V$ characteristics

An analysis of $I-V$ and $C-V$ characteristics, together with the calculated distribution of vacancies along the ion range (Fig. 1), shows their qualitative agreement. Indeed, simple representing the ion range as consisting of two regions, LDR and BPR, the region with a low current rise rate can be preliminary attributed to the SCR expansion from the p^+-contact into the LDR with a relatively low concentration of radiation defects. A subsequent sharp increase in current corresponds to the carrier generation that occurs when the SCR expands inside the BPR enriched with defects. These claims rely on the following relations.

— The concentration of primary vacancies is proportional to the fluence as

$$N_V(x) = g_V(x)F, \tag{1}$$

where $g_V(x)$ is the introduction coefficient of vacancies dependent of the coordinate x.

— The distribution of electrically active radiation defects with the concentration $N_t(x)$ along the ion range, which contribute to the bulk current, is defined by the $N_V(x)$ profile

$$N_t(x) = g_J N_V(x), \tag{2}$$

where g_J is the proportionality coefficient translating the vacancy concentration to the concentration of the current generation centers.

— The bulk generation current I_g arising in the SCR with a width W is

$$I_g = eSWU_g, \tag{3}$$

where e is the elementary charge, and U_g is the carrier generation rate at reverse bias voltage [12]:

$$U_g = \frac{\sigma_n \sigma_p \upsilon_{\text{th}} N_t n_i}{\tau_p \exp\left(\frac{E_i - E_t}{kT}\right) + \tau_n \exp\left(\frac{E_t - E_i}{kT}\right)} = \frac{n_i}{\tau_g}, \tag{4}$$

where E_t is the energy level of the current generation center in the silicon bandgap, σ_n and σ_p are the electron and hole capture cross-sections, respectively, E_i is the intrinsic Fermi level, υ_{th} is thermal velocity of electrons or holes, n_i is the intrinsic carrier concentration, τ_g is the carrier generation lifetime, and τ_n and τ_p are the lifetimes of electrons and holes, respectively, expressed as

$$\tau_{n,p} = \left(\sigma_{n,p} \upsilon_{\text{th}} N_t\right)^{-1}. \tag{5}$$

— The W dependence on V is expressed as

$$W = \frac{\varepsilon \varepsilon_o S}{C} = \left[\frac{2\varepsilon \varepsilon_o V}{eN_{\text{eff}}}\right]^{0.5}, \tag{6}$$

where ε and ε_o are the permittivity of silicon and vacuum, respectively. Then, the increase of the SCR width ΔW at raising the bias voltage to $V + \Delta V$ is

$$\Delta W = \frac{\varepsilon \varepsilon_o S}{C} = \left(\frac{\varepsilon \varepsilon_o}{2eN_{\text{eff}}}\right)^{0.5} V^{-0.5} \Delta V. \tag{7}$$

— The additional current density $\Delta J_g(W)$ generated in ΔW is

$$\Delta J_g(W) = eU_g(W)\Delta W, \tag{8}$$

where $U_g(W)$ is the carrier generation rate in the layer ΔW at $x = W$ defined by Eq. (4). Finally, the generation current density J_g in the entire SCR is the integral of U_g over W:

$$J_g = e \int_0^W U_g(x)dx. \tag{9}$$

The above relations enable to obtain the distribution of current-generating defects along the ion range from the experimental $I-V$ and $C-V$ characteristics, or to solve an inverse task, i. e., calculate the shape of $I-V$ characteristic at different F using Eqs. (4) and (7−9), the activation energy E_a of the generation current and the $W(V)$ dependence. In Fig. 4, solid lines, a series of $I-V$ characteristics is presented calculated by using the distribution of primary vacancies provided by SRIM (Fig. 1), the $W(V)$ dependence obtained from the experimental $C-V$ data via Eq. (6), and

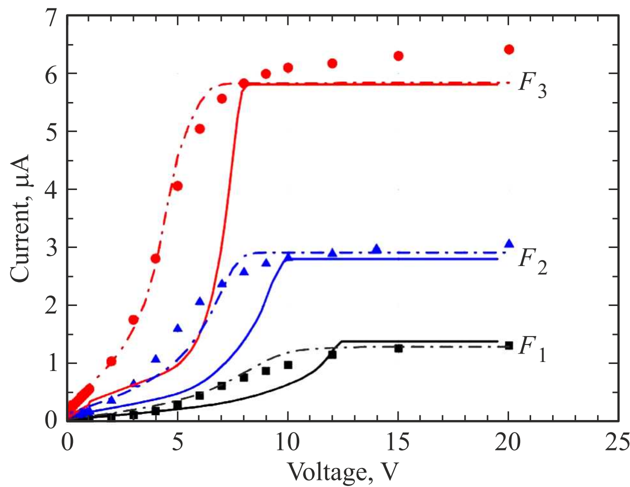

Figure 4. Comparison between experimental $I-V$ curves (symbols) and calculated $I-V$ characteristics obtained by using SRIM data (solid lines) and the model of two DAs (dash-dot lines).

the parameters derived in this study from the temperature dependence of the bulk current of diodes irradiated with 53.4 MeV ^{40}Ar ions, the activation energy of the generation current $E_a = 0.65$ eV and $\sigma_{n,p} = 8 \cdot 10^{-14}\,\text{cm}^2$; the latter were found to be the same as for Si detectors irradiated with hadrons [13]. Adjustment of the calculated current to the experimental one in the bias range 15–20 V corresponding to the current saturation yielded $g_J = 1.9 \cdot 10^{-2}$ in Eq. (2). It is consistent with the findings of many authors, e. g., in [14], that recombination of primary defects in the tracks reduces vacancy concentration contributing to the formation of electrically active defect complexes and clusters to about 2% relative to the initial concentration.

Comparison between the experimental $I-V$ data and the calculation showed their significant differences: a sharp increase in current in the experimental $I-V$ curves at significantly lower voltages than in the calculated ones, and an extended region of current transition from a sharp increase to saturation, which was not reproduced in the calculation. The difference can be explained by two factors:

— mismatch between the profiles of primary vacancies and electrically active centers generating the current due to the intensive formation of vacancy-related defects and clusters by ions at the range end;

— disregarding the diffusion component of the current, which delivers holes from the BPR to the p^+-contact through the nondepleted part of the damaged layer.

For estimating the contribution of the above factors, $I-V$ curves were calculated by using the program for numerical simulating the characteristics of semiconductor devices, which takes into account the full set of processes in reverse-biased diodes as described in [15]. Two acceptor levels, whose position is close to that observed in the DLTS and TSC spectra for Si detectors irradiated with hadrons [1,16], were involved in the simulation. The first one is the acceptor DA_1 positioned in the upper half of the silicon bandgap at $E_c - 0.47$ eV that corresponds to the activation energy of the generation current $E_a = 0.65$ eV, and this level does not affect N_{eff}. The second acceptor, DA_2, is the effective energy level that sums the impact of several radiation-induced defects. It is located in the lower half of the bandgap at $E_v + 0.47$ eV [13], that is close to that of cluster-related defect H152 K at $E_v + 0.42$ eV (the difference of 7%) [1,16]; the level compensates the charge of phosphorus donors N_0 and controls the electric field distribution $E(x)$ in irradiated diodes. Since for DA_1 and DA_2 the energy gaps that affect carrier generation have the same values of 0.65 eV, both levels act as the current generation centers, but give different contributions to the current. In the simulations, the distributions of both DAs were described by Eq. (2) with the coefficients g_J constant along r_p and individual for each defect. The results of simulation showed a much better fit to the experiment at $\sigma_{n,p} = 8 \cdot 10^{-14}\,\text{cm}^2$ reproducing a sharp current rise at $V < V_{fddr}$ and a subsequent gradual transition to its saturation (Fig. 4, dash-dot lines). It should be noted that for both simulations, the carrier cross-sections obtained in this study are at least 10–15 times greater than σ in the range 10^{-15}–$10^{-14}\,\text{cm}^2$ measured for relevant defects in the TSC spectra [1]. In turn, similar values of σ were defined earlier for effective current generation centers in Si detectors irradiated with hadrons, which agreed with the experimental data [13].

5.2. Electric field distribution in irradiated diodes

Fig. 5 shows the $E(x)$ profiles for irradiated diodes simulated with accounting for the nonuniform $N_V(x)$ distribution (Fig. 1) and using the above mentioned DA_1 and DA_2. For ease of presentation, in all curves the sign of the electric field is changed from negative (as follows from the Poisson equation [12]) to positive; negative gradient of the electric field, dE/dx, is the evidence of the SCR with positive N_{eff}, and vice versa. The sign of applied bias is negative at the p^+-contact.

Two features are observed in the profiles: a „bump“ within 10.5–14.5 μm at $V = 0$–5 V, and the region with the built-in field forming a junction around $x \sim r_p$. At $V = 0$ the curves demonstrate three extrema for all fluences (Fig. 5, a), e. g., at x of 12.7, 14.6 and 15.2 μm for the diode irradiated to F_3. For this diode, evolution of the profiles with increasing bias is presented in Fig. 5, b, which shows an expansion of the SCR from the p^+-contact into the damaged region; this region is denoted below as SCR_1 with the width W_1. The triangle in the $E(x)$ profiles around r_p evidences arising of an additional built-in junction with SCR_2 and the $E(x)$ maximum at $x \sim r_p$; SCR_2 extends inside LDR from $x \sim r_p$ towards the p^+-contact, and in NDR as well. The dE/dx is positive at $x < r_p$ (negative concentration of charged DAs compensates for N_0), whereas in the NDR dE/dx is negative and corresponds to N_0. At $x < r_p$ and $V = 0$, the electric field in the SCR_2 drops

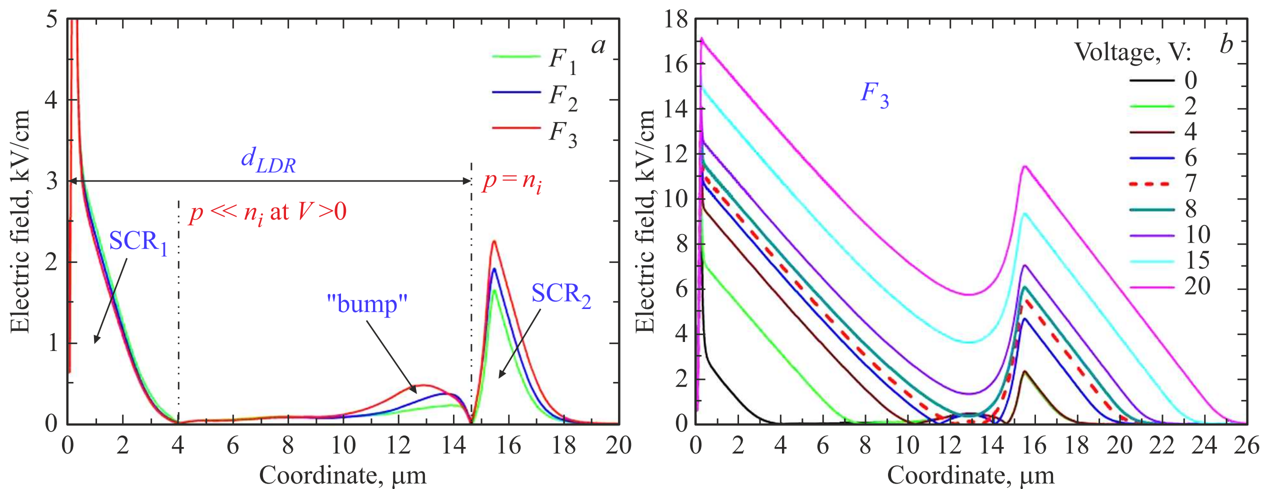

Figure 5. Simulated profiles of the electric field in irradiated Si diodes: *a*) $V = 0$, different F, and *b*) F_3, different V.

sharply and reaches its local narrow minimum with $E \sim 0$ at $x = 14.6\,\mu$m, in which N_{eff} is zero and $n = p = n_i$. Therefore this coordinate can be considered as the boundary between the LDR and BPR, and the relevant width of LDR, d_{LDR}, extends from $x = 0$ to $x(E = 0)$. This width is practically independent of F and only slightly affected by the voltage in the range $0-7$ V.

At $x < d_{\text{LDR}}$, the $E(x)$ profile translates into a bump, which also shows dE/dx with different signs (positive on the left and negative on the right, respectively) around a smooth maximum. It should be noted that the electric field minimum and the bump are observed in a limited voltage range, and at $V > 7$ V, when the SCR_1 boundary approaches the BPR, merging of SCR_1 and SCR_2 takes place, and the $E(x)$ profiles represent the curves with two maxima, at the p^+-contact and $x \sim r_p$ (Fig. 5, *b*). The profiles hold this shape at V higher than the voltage of the current saturation of 7 V and are determined by the difference in the concentrations of shallow donors and deep acceptors along the ion range.

These features in the $E(x)$ profiles nicely agree with $C-V$ and $I-V$ characteristics of irradiated diodes. Expansion of SCR_1 corresponds to the decrease in capacitance in the range of $0.5-5$ V (Fig. 2). Compensation of N_0 is visualized in the $C-V$ curves for the diodes irradiated to F_2 and F_3 as a region at $V = 5-10$ V with a successive reduction in capacitance and its further rise. For the diode irradiated to F_3, merging of two electric field regions takes place at $V \sim 8$ V, which corresponds to the current saturation (Fig. 3). For the diodes irradiated to F_1 and F_2, saturation occurs at higher V, which agrees with a smaller concentration of compensating DAs.

5.3. Contribution of hole diffusion to the current of irradiated diodes

The $E(x)$ profiles for the diode irradiated to F_3 show that within the range $V = 0-7$ V two regions are observed in the damaged bulk, whose boundaries are the coordinates with fixed concentrations of free carriers. The first is the LDR part, in which the $E(x)$ profile varies, and the hole concentration changes from $p(x = W_1) = 0$ to $p(x = d_{\text{LDR}}) = n_i$, while the coordinate $x(E = 0)$ shifts and d_{LDR} reduces with raising the bias. The second is the region from $x = d_{\text{LDR}}$ to $x \sim r_p$, in which at $V > 8$ V the hole concentration decreases from n_i to the concentration in the BPR dependent of V and F. A condition $p = n_i$ at $x = d_{\text{LDR}}$ in the range $V = 0-7$ V enables estimating the contribution of the diffusion current I_{dif} in LDR to the total current via the average hole gradient $n_i/(d_{\text{LDR}}-W_1)$ as

$$I_{\text{dif}} = eD_p \frac{n_i}{d_{\text{LDR}} - W_1}, \tag{10}$$

where D_p is the hole diffusion coefficient.

For the diode irradiated to F_3, estimation of J_{dif} flowing out of the LDR gives $17\,\mu\text{A/cm}^2$ at $V = 1$ V, $W_1 = 6\,\mu$m, $d_{\text{LDR}} = 14.5\,\mu$m, $n_i = 5.6 \cdot 10^9\,\text{cm}^{-3}$ ($T = 293$ K), and $D_p = 16\,\text{cm}^2/\text{s}$, which is 6.7 times greater than the experimental J of $2.5\,\mu\text{A/cm}^2$ recorded at the same V (Fig. 3). For $V = 6$ V, W_1 is $12\,\mu$m, while d_{LDR} is the same as at $V = 1$ V, and J_{dif} is $57\,\mu\text{A/cm}^2$, whereas the measurements show $J \approx 22\,\mu\text{A/cm}^2$.

In turn, disregarding the features related to the nonuniform defect distribution in the LDR allows estimating the diffusion current density $J_{\text{dif_st}}$ by using a standard expression:

$$J_{\text{dif_st}} = \frac{eD_p p_n}{L_p}, \tag{11}$$

where $p_n \approx (n_i)^2/N_0$ and L_p are the concentration and diffusion length of holes, respectively; the latter is defined as

$$L_p = \sqrt{D_p \tau_p}, \tag{12}$$

where the hole lifetime τ_p is

$$\tau_p = (\sigma_p v_{\text{th}} N_t)^{-1}. \quad (13)$$

For the diode irradiated to F_3, at $x < 10\,\mu$m the mean values are $p_n = 4.4 \cdot 10^7\,\text{cm}^{-3}$ and $\tau_p = 1\,\mu$s, which yields $J_{\text{dif_st}} = 28\,\text{nA/cm}^2$ that is too small to justify the experimental current.

The difference between the diffusion current estimate J_{dif} and the experimental data, on the one hand, and the agreement between the simulated and experimental $I-V$ characteristics (Fig. 4), on the other hand, should be attributed to a simplified approach to evaluating the hole concentration gradient in the LDR in Eq. (10) as a constant inside the region $[W_1; d_{\text{LDR}}]$, thereby leading to J_{dif} overestimation. Apparently, in this range there is an extended region with a low gradient, which controls the hole flow to the SCR_1 boundary. Meanwhile, the approach gives a qualitatively correct ground for the rise in this component with voltage due to the decrease in the layer thickness $(d_{\text{LDR}}-W_1)$ within the bias range 0−7 V, in which the concentration of holes at the LDR/BPR boundary stays constant and equals n_i. Further rise in voltage above 7 V leads to the increase in electric field and the hole concentration reduction at the boundary. The concentration of holes in the nondepleted BPR reduces due to a more efficient hole outflow from the BPR, and the rate of carrier transition U in this region changes in accordance with the Shockley-Reed Hall statistics as [12]

$$U = \frac{\sigma_p \sigma_n v_{\text{th}} N_t (pn - n_i^2)}{\sigma_n \left[n + n_i \exp\left(\frac{E_t - E_i}{kT}\right)\right] + \sigma_p \left[p + n_i \exp\left(\frac{E_i - E_t}{kT}\right)\right]}. \quad (14)$$

As free carrier concentrations in the BPR and hence np go down, U increases, which leads to the current rise to the maximum and further saturation, starting before the SCR_1 boundary reaches the coordinate of the defect concentration maximum inside the BPR.

Finally, the current-related damage factor α can be estimated as [8]

$$\alpha = \frac{\Delta I}{F V_{\text{DR}}}, \quad (15)$$

where ΔI is the increase in current over the whole volume of the damaged region, $V_{\text{DR}} = r_p S$, and ΔI are taken from Fig. 3. The $\Delta I(F)$ dependence is linear, and its slope yields $\alpha = 3.9 \cdot 10^{-12}$ A/cm, which is almost 5 orders of magnitude greater than that for hadrons. At the same time, it is in a reasonable agreement with the result $\alpha = 4.9 \cdot 10^{-12}$ A/cm for ^{40}Ar ions with a lower energy of 20 MeV [7], since the average displacement production rate decreases with the particle energy rise.

6. Summary

The study of $I-V$ characteristics of Si diodes irradiated with short-range 53.4 MeV ^{40}Ar ions creating nonuniform defect distribution with the Bragg peak region enriched with defects was performed via processing the experimental $I-V$ and $C-V$ data and simulating the $I-V$ characteristics and the electric field profiles by using acceptor-type radiation-induced defects.

It was shown that considering the dark current in terms of the carrier thermal generation in the depleted region, which is valid for Si detectors irradiated with hadrons, fails in describing the $I-V$ curves of diodes irradiated with short-range ions. The reason is that high local concentration of deep acceptors in the BPR forms an additional junction around the ion range end. The junction controls hole diffusion and leads to the sharp rise in the total current at bias voltages less than the full depletion voltage of the damaged region, while the saturation current is determined by the nuclear energy loss of ions in silicon.

The suggested model of diffusion current flow from the damaged region is self-consistent in terms of the mechanisms and quantitative description of $I-V$ characteristics of Si diodes irradiated with short-range ions. The $E(x)$ profile in the sensitive region of Si sensors is controlled by the BPR, which should be taken into account while predicting radiation degradation of the sensor signal.

The paradox of the large carrier capture cross-sections close to $10^{-13}\,\text{cm}^2$ for the current generation centers known earlier for Si detectors irradiated with hadrons is revealed also for Si diodes irradiated with short-range ions. These values nicely agree with the experimental results on the bulk current in Si sensors irradiated with both types of particles.

Funding

This study was supported by a financial subsistence of the Ministry of Science and Higher Education of Russian Federation (state project № 0040-2019-0024).

Conflict of interest

The authors declare that they have no conflict of interest.

References

[1] M. Moll, IEEE Trans. Nucl. Sci. **65**, 1561 (2018).
[2] Chiara Grieco, Sebastian Grinstein, Salvador Hidalgo, Giulio Pellegrini, David Quirion, Stefano Terzo, Nucl. Instrum. Meth. A **979**, 1 November 2020, 164458.
[3] *Development of physics and technology of charged particle accelerators,* complier editors B.Yu. Sharkov and I.N. Meshkov (M., RAS, 2021). ISBN 978-5-907366-27-5 (in Russian).
[4] L.V. Grigorenko, B.Y. Sharkov, A.S. Fomichev et al. Physics — Uspekhi **62** (7) (2019). DOI: https://doi.org/10.3367/UFNe.2018.07.038387 (in Russian).
[5] *Material Science with Ion Beams, Topics in Applied Physics,* **116** (2010), Harry Bernas Eds. (Springer; Berlin, Germany).
[6] V. Eremin, D. Mitina, A. Fomichev, O. Kiselev, N. Egorov, I. Eremin, A. Shepelev, E. Verbitskaya, J. Instrum. **13**, P01019 (2018).

[7] M. Kurokawa, T. Motobayashi, K. Ielu, S. Shimoura, H. Murakami, Y. Ikeda, S. Moriya, Y. Yanagisawa, T. Nomura, IEEE Trans. Nucl. Sci. **42**, 163 (1995).
[8] E. Fretwurst, N. Claussen, N. Croitoru, G. Lindström, B. Papendick, U. Pein, H. Schatz, T. Schulz, R. Wunstorf, Nucl. Instrum. Meth. A **326**, 357 (1993).
[9] J.F. Ziegler, J.P. Biersack, M.D. Ziegler, 2008, The Stopping and Range of Ions in Solids, http://www.srim.org/
[10] Z. Li, H.W. Kraner, IEEE Trans. Nucl. Sci. **38** (2), 244 (1991).
[11] E. Borchi, M. Bruzzi, S. Pirollo, S. Sciortino, Solid State Electron. **42** (11), 2093 (1998).
[12] S.M. Sze, K.K. Ng, *Physics of semiconductor devices,* 3rd edition (J. Wiley & Sons, Inc., Hoboken, New Jersey, 2007).
[13] E. Verbitskaya, V. Eremin, I. Ilyashenko, Z. Li, Nucl. Instrum. Meth. A **754**, 63 (2014).
[14] Victor Van Lint, Nucl. Instrum. Meth. A 253, 453 (1987).
[15] E. Verbitskaya, V. Eremin, A. Zabrodskii, P. Luukka, J. Instrum. **11**, P12012 (2016).
[16] I. Pintilie, G. Lindström, A. Junkes, E. Fretwurst, Nucl. Instrum. Meth. A **611**, 52 (2009).